



Multi-channel surface NMR instrumentation and software for 1D/2D groundwater investigations

David O. Walsh*

Vista Clara Inc., 2615 West Casino Road, Suite 4-JK, Everett, WA 98204, USA

ARTICLE INFO

Article history:

Received 31 January 2007

Accepted 28 March 2008

Keywords:

Surface nuclear magnetic resonance

Surface NMR

SNMR

Magnetic resonance imaging

MRI

GeoMRI

Multi-channel

MRS

Magnetic resonance sounding

Magnetic resonance tomography

ABSTRACT

Multi-channel surface nuclear magnetic resonance (NMR) instrumentation and software, developed in the United States, has been applied to investigate 1D and 2D hydrology at various locations in the Western US. The GeoMRI instrument offers several practical improvements over the previous state of the art in surface NMR instrumentation, including a multi-channel transmit/receive capability, a significantly shorter measurement dead-time of 10 ms, and an ultra-low receiver input noise density of less than 0.4 nV/sqrt (Hz). Two multi-channel NMR processing techniques, reference coil-based noise cancellation and integrated FID imaging, are shown to increase effective signal to noise ratios by an order of magnitude or more. These effective SNR gains enable multi-coil surface NMR to produce useful and reliable images when the post-averaged SNR is less than 1. We also suggest an alternate approach to imaging, in which NMR signals are initially isolated in the space domain, and then NMR parameter estimation is applied in the time domain. Experimental results are presented for recent surface NMR groundwater investigations conducted in Nebraska and Texas, USA.

© 2008 Elsevier B.V. All rights reserved.

1. Introduction

Single-channel surface NMR instruments have been commercially available for about 10 years. To date, their widespread use in hydrogeological investigations has been limited by their susceptibility to environmental and cultural noise, and their limitation to groundwater profiling in a single dimension: depth.

Susceptibility to noise continues to pose the primary obstacle to the widespread use of surface NMR for hydrological investigations (Legchenko, 2006). Notch filtering, aimed at zeroing the response to 50 Hz or 60 Hz power transmission harmonics, is the most common method of reducing noise in surface NMR measurements (Legchenko and Valla, 2003). A recent experimental study by Legchenko (2006) indicated that narrowband 50 Hz power harmonics represent only 20% to 50% of the total noise energy in a typical band-limited surface NMR measurement, while broadband non-stationary noise processes typically constitute a majority of the noise energy. Notch filtering may also distort the underlying NMR signal when the Larmor frequency is close to a multiple of 50 Hz or 60 Hz. Other noise reduction techniques have been proposed for detecting and removing impulse-like noise processes from surface NMR data (Li et al., 2006, Strehl et al., 2006). It makes sense to remove high-amplitude impulse noise artifacts from NMR data. When the density of impulse noise artifacts is high, re-

moval of entire data records can increase the data collection time significantly, possibly by several integer factors. Removing only the affected portion of each data record will distort the underlying NMR signal unless more sophisticated processing is employed to reconstruct the lost portion of the desired NMR signal.

The use of a “figure-8” shaped surface coil is a simple and commonly employed form of spatial noise mitigation, and is often effective when the noise field is homogeneous across the coil surface. The “figure-8” coil shape alters the transmitted field pattern however, and significantly reduces the maximum depth of investigation compared to a circular or square surface coil. A modification to this method is the use of a displaced reference coil with reverse polarity, wired in parallel to the detection coil, with a passive diode-based switch to prevent current from flowing through it during the transmit pulse (Lange et al., 2006). This single-channel configuration acts as a conventional coil during transmit (for maximum depth of penetration) and acts like a figure-8 coil in receive mode, canceling the magnetic flux common to both coils. The modified figure-8 loop exhibits lower sensitivity to signals at larger depths in receive mode. Both the standard and modified configurations of the figure-8 loop operate by canceling the magnetic flux common to both coils. Their effectiveness depends on the homogeneity of the magnetic noise process across the coils. Such homogeneity is often limited in the vicinity of human development, and in situations with multiple competing noise sources (power line harmonics, electric fences, sferics, etc...).

Multi-channel surface NMR instrumentation enables the use of multiple, independent reference coils for space-based noise mitigation. The potential advantages of spatial or space/time processing

* Tel.: +1 425 290 3626; fax: +1 707 982 1799.

E-mail address: davewalsh@vista-clara.com.

include: no distortion of the underlying NMR signal (subject to proper placement of reference coils) and no requirement for noise process models. The use of separate receive channels for reference coils preserves all the spatial noise cancellation advantages of the figure-8 and modified figure-8 methods, and provides the additional degrees of freedom necessary to mitigate a plurality of interfering EM noise processes with differing temporal/spatial characteristics in a time/space inhomogeneous noise environment through adaptive signal processing (Haykin, 1996).

The development of multi-channel surface NMR instrumentation also facilitates time- and energy-efficient 2D and 3D groundwater imaging methods. Preliminary computer modeling by Hertrich and Yaramanci (2003) indicated that 2D surface NMR imaging with separated transmitter and receiver loops is feasible, and yields improved spatial resolution compared to 2D imaging with a single coincident transmit/receive loop processed over multiple displaced stations. Hertrich et al. (2005) conducted a 2D surface NMR field survey using a single-channel surface NMR instrument, by repeated soundings using all possible permutations of 4 transmit/receive coil locations (i.e. 16 separate soundings to generate a four-coil transmit/receive array data set), and concluded that multi-channel surface NMR instrumentation would enable superior 2D investigations at feasible survey speeds (Hertrich and Yaramanci, 2006).

The feasibility of 3D surface NMR groundwater investigations was investigated and demonstrated by Walsh (2006). Computer modeling demonstrated the ability to resolve a 3D target using an array of four circular surface coils laid out in a square pattern on the surface (approximate 10% overlap between adjacent coils). The feasibility of 3D surface NMR imaging was experimentally validated through laboratory surface NMR imaging experiments, conducted in the boosted B_0 field of an 8 ft × 8 ft × 4 ft Helmholtz coil (Walsh, 2006). In these experiments a rectangular container of mineral oil was imaged in three dimensions using an array of four small (43 cm diameter) multiple-turn surface coils, with resulting spatial resolution similar to the respective computer modeling (Walsh, 2006).

In this work, we describe the development of multi-channel surface NMR instrumentation and software, and their application to noise reduction and 2D NMR groundwater imaging. The GeoMRI instrument and the multi-channel surface NMR applications described herein were developed by Vista Clara Inc. over the past 4 years, with funding from the US National Science Foundation. The author was the principal investigator on the instrument development effort, but other employees, consultants and subcontractors played key roles in the development effort.

In this paper we outline the technical specifications and capabilities of the GeoMRI instrument. We demonstrate effective reduction of environmental noise using reference coils with adaptive signal processing. We introduce an integrated FID imaging method, which is useful for groundwater NMR imaging when the post-averaged signal to noise ratio (SNR) is less than 1. Finally, we present the results of some recent 1D and 2D groundwater investigations conducted in the United States.

2. Methods

2.1. Instrumentation

The field studies described in this paper were performed using the "GeoMRI" surface NMR instrument shown in Fig. 1. All power components are housed in one enclosed unit, which is installed in a small convertible cargo trailer. The GeoMRI instrument produces maximum AC current pulses in excess of 400 A, with a maximum of 4000 V across the coil terminals. The instrument has a DC bus capacitance of 0.24 F, which enables multiple-pulse sequences (e.g. spin-echo or 90–90°) with minimal voltage and current drop between pulses. The surface coils are constructed of #8 AWG stranded tinned copper



Fig. 1. GeoMRI, 4-channel surface NMR instrument (April 2006).

(approximate cross-section of 10 mm²), with 15 kV DC insulation, high voltage MilSpec environmental-rated connectors, in individual sections of 300 ft (91 m) length.

The GeoMRI instrument has a software selectable Tx/Rx dead-time of 10 ms or 15 ms, and is capable of measuring signals within 5 ms of the end of the transmit pulse. This shortened instrumentation dead-time provides for higher SNR and more accurate estimation of free induction decay (FID) properties (specifically initial amplitude and T2*), especially for the shortest duration FID signals. The author is presently investigating the utility of shorter dead-times for the detection of silt-bound water, detection of water in magnetically permeable formations, and detection of capillary-bound water.

The GeoMRI system has 4 transmit/receive channels, allowing the system to transmit on one or multiple coils at the same time, and simultaneously receiving NMR data on up to four receive channels. The analog input circuitry has a bandwidth of approximately 10 kHz, and raw NMR data are directly digitized using 24-bit A/D's with zero time delay between channels. This broadband sampling approach preserves the broadband information content of the measured NMR signals, and the 24 dB dynamic range leaves plenty of headroom for the measurement of broadband noise and interference sources, which may be filtered out during post-processing as needed. Timing and phase jitter between successive measurements, and between channels, are negligible. The absolute phase offset of the input electronics has not been assessed, although it would be a straightforward procedure to calibrate any receiver-induced phase offset.

The receive electronics are designed to present a high impedance to each surface coil, to suppress mutual coupling between adjacent surface coils. An important aspect of this design is that the surface coils are not tuned in receive mode, as the use of parallel tuning capacitors would create low-impedance circuits enabling currents to flow freely through the coils in receive mode. Mutual coupling between surface coils, if not suppressed, will cause mixing of the signals amongst all coils in the receive array, and greatly complicate the problem of modeling and inverting NMR signal distributions in one or multiple dimensions. The absence of tuning capacitors in receive mode also eliminates the gain and phase response ambiguities associated with tuned surface loops.

The receiver open-circuit input noise is 0.4 nV/sqrt (Hz) at 2 kHz. This noise figure was measured in a noisy laboratory environment with the measured coil terminals left open, and the instrument powered on and transmitting through a coil connected to an adjacent Tx/Rx channel. Hence, this noise measurement includes the accumulated effects of all instrumentation and digitization noise. This ultra-

low measurement noise floor is significant to the prospects for small-scale multi-channel surface NMR in the Earth's magnetic field.

2.2. Adaptive noise cancellation

One or more surface coils may be used as reference sensors to measure the ambient noise or interference. The GeoMRI system software includes proprietary adaptive signal processing algorithms based on correlation cancellation (Haykin, 1996), which process the data from one or more reference coils to adaptively cancel noise on the detection channels. For maximum effect, the reference coils should be employed in a manner to maximize detection of the local noise processes, while minimizing inadvertent detection of the NMR signal. In practice, this means moving the reference coils away from the detection coils and preferably towards known noise sources, and/or using reference coils with smaller diameters to reduce sensitivity to the groundwater at greater depths.

Through experience, Vista Clara Inc. has developed a practice of separating the noise reference coil(s) from the detection coil(s) by a length of at least one detection coil diameter, whenever feasible. This recommended separation is given as an edge-to-edge distance, so the centers of the detection and reference coils are separated by a somewhat larger distance. A noise survey with a portable noise measurement device is often helpful in determining the spatial character of the noise gradient(s), and the best initial placement of reference coils at a particular site. In the author's experience, it sometimes necessary try several different reference coil arrangements to obtain the best possible noise cancellation results at a given site. It is also the author's experience that it is usually worth the extra effort to get the reference coil(s) emplaced in a favorable geometry, as effective noise cancellation can often improve the SNR by a factor of 10 or more.

2.3. Imaging algorithms

Imaging is the process of localizing and separating the NMR signals from different locations in the 1D, 2D or 3D volume of investigation. In our processing scheme, imaging is always applied first to isolate the NMR signal emanating from a particular depth interval (1D imaging) or a particular volume element (2D or 3D imaging). NMR signal parameter estimation, such as exponential model fitting and hydrologic characterization, are performed after the localized NMR signals have been isolated via the imaging procedure.

This imaging approach, localizing the NMR signals first, and then estimating the NMR and hydraulic parameters based on localized NMR signals, represents a notable departure from previously published surface NMR inversion methods (Legchenko and Shushakov, 1998; Hertrich et al., 2005; Mohnke and Yaramanchi, 2005). The conventional 1D inversion approach involves first fitting an exponential model(s) to the post-averaged (stacked) time series at each pulse moment to estimate the amplitude, decay time(s), frequency and phase, and then uses the kernel function to derive spatially-dependent NMR and hydraulic parameters (water content, time decay, etc...). We provide no direct comparison to the conventional inversion approach here.

2.3.1. Linear pseudo-inversion

The imaging process described here involves modeling the groundwater signal source as a finite set of voxels spanning the 3D subsurface volume of investigation. The NMR signal and decay properties are assumed to be uniform within each voxel, and the individual coil B1 vector fields are calculated at the centroid of each voxel and modeled as uniform throughout each voxel. A set of linear equations is developed to relate the contributions from individual voxels to the set of recorded multi-coil surface NMR signals.

For 1D inversion with a single coincident loop, assuming an insulating Earth model, the transverse coil vector fields are calculated at

the centroid of each voxel, and the forward equations are formulated as follows:

- 1) A set of finite 1D layers are selected, and the NMR-detectable water content $W_{\text{NMR}}(z)$ and relaxation properties are assumed constant throughout each 1D layer. Each layer is modeled as a 2D set of volume elements, with constant water content and relaxation properties throughout each volume element. This finite element approach incorporates the variability of the coil fields throughout each layer.
- 2) For each vertical layer, and each transmitted pulse moment q , the hypothetical contribution to the receive coil voltage due to the processing bulk magnetic moment M_{xyz} in each voxel is calculated as:

$$dV(q, x, y, z) = \omega_L \cdot |B_R(x, y, z)| \cdot |M_{xyz}| \cdot \sin(\theta) \quad (1)$$

$$\theta = \frac{q\gamma|B_R(x, y, z)|}{2}, \quad q = I_0 T_{\text{pulse}} \quad (2)$$

where M_{xyz} is calculated on the basis of 100% water content within the voxel and $B_R(x, y, z)$ is the transverse component of the coincident coil B1 field.

- 3) The modeled coil voltage for the entire layer is the sum total of the (real) contributions from the individual voxels in that layer:

$$K(q, z) = \sum_{x,y} dV(q, x, y, z). \quad (3)$$

- 4) The forward matrix K , is thus constructed for all values of transmitted pulse moment q , and all hypothetical water layers with centroids at depths z .
- 5) The matrix K is inverted directly, using its singular value decomposition (SVD), and regularized in the process by eliminating the singular vectors with corresponding singular values below a user-selected threshold. A regularized pseudo-inverse of the forward matrix K may be computed via other direct methods, or via linear iteration (i.e. the gradient-descent algorithm, Haykin, 1996). To simplify the discussion, we refer to the regularized pseudo-inverse of K as H .
- 6) The post-averaged measured NMR signals are arranged as rows in a data matrix V , and the normalized sampled NMR signals corresponding to the water content in the N_z layers are isolated via multiplication of the pseudo-inverse H and the data matrix V

$$W_{N_z \times N} = H \cdot V \quad (4)$$

where the m th row of W is the normalized signal from the m th layer in the 1D model.

The time-domain NMR signals, "isolated" into contributions from individual layers by the procedure above, are amplitude-normalized with respect to a water content of 100%, and retain the time decay characteristics of the underlying NMR signals in that layer. Of course spatial resolution and accuracy depend upon the degree of regularization, spatial sampling resolution, and generally the accuracy of the assumptions used to derive the B1 coil fields and the discretized volume 3D source model.

For 2D or 3D inversion with separated transmit and receive loops, the recorded (post-averaged) time-domain signals are initially demodulated to baseband by multiplication with the sampled complex exponential function $d(n)$:

$$d(n) = 2e^{-j\omega_0 nT} \quad (5)$$

and low-pass filtered to remove the component at $2\omega_0$. The signal space is discretized into a finite set of 3D voxels, whose water content and relaxation properties are assumed fixed in within each voxel (3D imaging) or along one dimension (2D imaging). The transverse coil fields are calculated at the centroid of each voxel,

and Eqs. (1) and (2) are generalized to the case of separated transmit and receive loops:

$$dV(q, x, y, z) = \omega_L \cdot |B_R(x, y, z)| \cdot |M_{xyz}| \cdot \sin(\theta) \cdot e^{i\phi_R} \quad (6)$$

$$\theta = \frac{q\gamma|B_T(x, y, z)|}{2}, \quad q = I_o T_{pulse} \quad (7)$$

where M_{xyz} is calculated on the basis of 100% water content within the voxel. The receive phase offset ϕ_R is the phase of the NMR signal observed on the receive coil relative to the transmit coil current, and is determined by the geometrical angle between the transverse components of the transmit and receive coil fields at the voxel in question, as well as the direction of precession of the magnetic moment about the static field B_0 .

In cases where electrical conductivity profiles are available, the transverse coil fields at each voxel may be calculated using whatever forward model is available. If an advanced model incorporating elliptical polarization and conductivity-induced phase effects is available (Braun et al., 2005), then the Eqs. (1), (2), (6) and (7) may be expanded into the generic kernel function for separated transmit/receive loops in conductive media (Hertrich et al., 2005).

2.3.2. Linear correlation

We have also found that linear correlation can sometimes provide useful spatial resolution. A spatial matched filter $S(:, z)$ for the NMR processes at depth z , is constructed by normalizing each row of the kernel function K

$$S(:, z) = \frac{K(:, z)}{\|K(:, z)\|}. \quad (8)$$

The spatial matched filter is correlated against the NMR data in the q domain, isolating a normalized version of the NMR signal from each depth interval through linear correlation

$$W_{N_z \times N} = S \cdot V. \quad (9)$$

We have found correlation-based imaging useful in cases where we are able to produce a large spread of tip angles throughout the volume of interest, and hence where the large spread of tip angles vs. pulse moment is sufficient to de-correlate the signals emanating from different 1D, or 2D locations in the subsurface. These de-correlation conditions are favored by the application of larger current pulse amplitudes, smaller loop diameters, and 2 or more loop turns in series.

2.4. NMR parameter estimation

Once localized into contributions for individual layers or voxels, the time-domain NMR signals are processed using linear or non-linear least-squares estimation procedures to fit one or more exponential models. For 1D inversions with coincident Tx/Rx loop, the localized NMR signals at this stage are real. For 2D or 3D inversions, the localized NMR signals are complex and at baseband. The mono-exponential fitting procedure returns estimates of the following parameters for each localized NMR signal: initial amplitude (directly interpreted as water content by volume fraction), $T2^*$ time decay, frequency, phase, and the time-domain integral of the FID signal which is useful for estimating permeability in low-SNR conditions (see discussion below). A multi-exponential fitting algorithm has also been implemented to estimate the water content distribution as a function of $T2^*$, for each layer or voxel. The multi-exponential fitting algorithm fits a set of exponentials with predetermined $T2^*$ decay rates (Mohnke and Yaramanci, 2003), and enforces a non-negativity constraint on the resulting amplitude distribution.

2.5. FID integration for permeability imaging

In many cases where the SNR is too low to produce reliable 1D or 2D estimates of NMR-detectable water content Φ and $T2^*$, a reliable

estimate of their product $P=\Phi T2^*$ may be estimated as the time-domain integral of the localized FID signal $g(n)$

$$\hat{P} = \left(\frac{1}{f_s} \right) \cdot \sum_n g(n), n = 0, \dots, N - 1 \quad (10)$$

where f_s is the sampling frequency, and $g(n)$ is the sampled, demodulated, normalized NMR signal localized through the imaging procedure described above to an individual 1D layer or 2D/3D voxel.

We derive this estimate as follows. Assume the detected and demodulated NMR signal due to processing protons in the voxel in question takes the following form:

$$g(t) = E_o \exp(-t/T2^*), t > 0. \quad (11)$$

The time-domain integral of Eq. (11) is

$$A = \int_{T_D}^{T+T_D} E_o \exp(-t/T2^*) dt = (E_o T2^*) \cdot \exp(-T_D/T2^*) \cdot (1 - \exp(-T/T2^*)) \quad (12)$$

where T_D is the instrument measurement “dead-time” between the end of the transmit pulse and the start of data recording, and T is the recording time. The equivalent estimate of P for sampled signals in Eq. (10) substitutes a finite sum for the finite integral, and incorporates the normalization effect of the imaging procedure, which equates the initial signal amplitude E_o to the NMR-detectable water content Φ .

2.5.1. Approximation error

Note that the integral A underestimates the product $E_o T2^*$ by a factor related to the instrument dead-time, the measurement time, and the time decay constant. If the measurement time T is long compared to $T2^*$ (in effect, if $T > 3 T2^*$) then the third term in Eq. (12) is approximately 1. If the dead-time T_D is short compared to $T2^*$ then the second term in Eq. (12) also approaches 1. For the typical GeoMRI experimental parameters $T_D=10$ ms and $T=2$ s, and a typical permeable fine-medium sand aquifer with $T2^*=100$ ms, the finite sum of Eq. (10) underestimates the actual product $P=\Phi T2^*$ by about 10%.

2.5.2. Relation to hydraulic conductivity

The dependence of permeability on porosity and the NMR relaxation rate (specifically $T2$) has been studied intensively in the petrophysical field for two decades. Two generic formulations have been traditionally used in borehole NMR applications, the Timur-Coates equation (Allen et al., 2000):

$$k_{TC} = a\phi^m (\text{FFV}/\text{BFV})^n \quad (13)$$

where FFV is the free-fluid volume and BFV is the bound fluid volume, and the Schlumberger-Doll Research equation (Allen et al., 2000; Kenyon and Gubelin 1995):

$$k_{SDR} = b\phi^m (T_{2LM})^n \quad (14)$$

where T_{2LM} is the logarithmic mean of the continuous T_2 relaxation distribution. In Eqs. (13) and (14) the exponents are typically $m=4$ and $n=2$, but can vary with local conditions (Allen et al., 2000). The lithology-dependent constant b in Eq. (14) is highly variable in itself, typically 4 for sandstones and 0.1 for carbonates (Kenyon and Gubelin, 1995). Early published work (Sen et al., 1990) supported the use of $m=4$ and $n=2$ for the case of borehole measurements on double porosity sandstones.

Earlier work by Kenyon (1992) established that permeability in consolidated sediments is dependent on both Φ^2 and T_2^2 . More recently, it has been observed that the sum of all spin-echo amplitudes in a CPMG sequence is proportional to the product of porosity and the average T_2 (Sezginer et al., 1999), and that this product correlates well

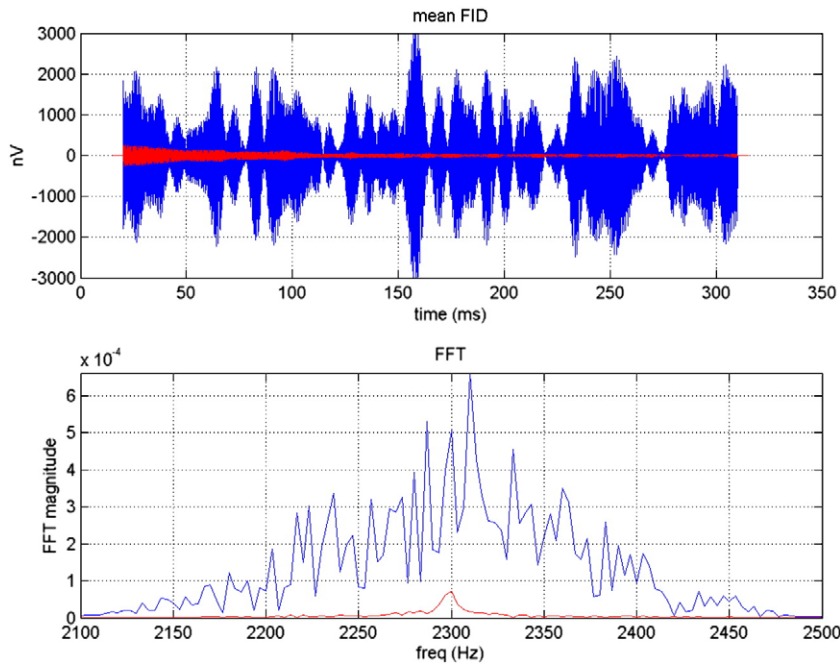


Fig. 2. Surface NMR signal and noise acquired near a large feedlot (USGS site 38), in central Nebraska, USA, April 2007. Shown are the mean FID averaged over 64 individual data records with different pulse moments (top), and its frequency spectra (bottom). Blue: NMR signal before noise cancellation. Red: NMR signal after adaptive noise cancellation using two reference coils.

with permeability (Sezginer et al., 1999). This sum of echo amplitudes has the additional advantage of high signal-to-noise ratio, and the technique is now routinely used in borehole NMR logging to obtain high-speed/high-resolution estimates of permeability.

Note that the sum of echo amplitudes technique for borehole NMR-based permeability estimation is highly analogous to the FID Integration method proposed here for surface NMR-based permeability estimation. Both techniques use time-domain integration estimate the area under the measured relaxation curve. Both techniques produce an estimate of the product of porosity and T_2 or T_2^* relaxation, and this product has been empirically related to permeability in the borehole application.

Lastly and most importantly, both methods can reliably estimate this product in low-SNR conditions that would preclude reliable NMR-based estimation of the porosity and T_1 or T_2^* , and hence permeability.

There has also been considerable research into the use of surface NMR for permeability estimation. This research is largely based on developing empirical relationships between the NMR-based estimates of free water content ϕ_{NMR} and T_1 or T_2^* relaxation rates, and measured permeability. The resulting mathematical models have tended to follow the form of Eq. (14), with the exponential factors m and n ranging between 1 and 4, depending on the experimental data and methods used to develop the empirical relationships.

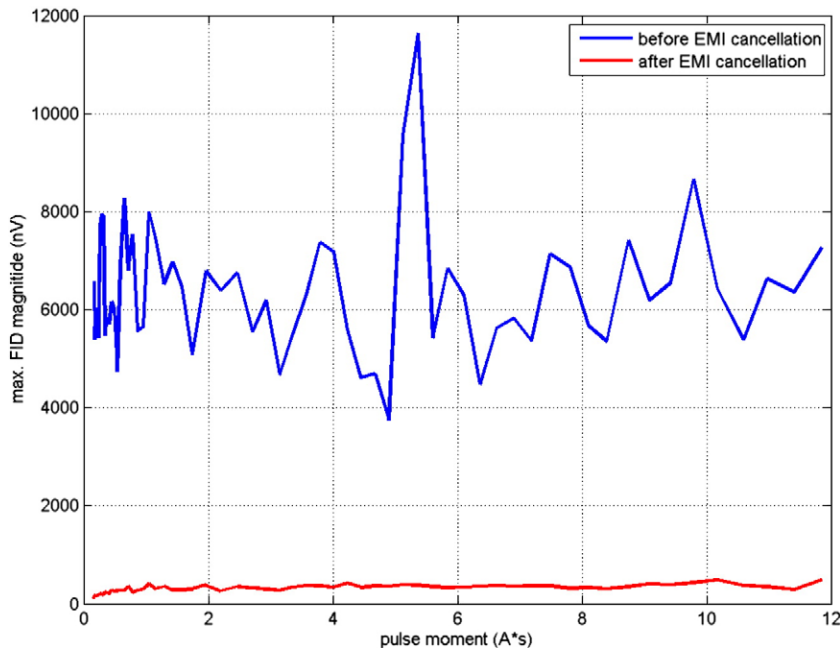


Fig. 3. Maximum signal magnitude vs. pulse moment for USGS site 38 (the feedlot site) in central Nebraska, USA, April 2007. Blue: NMR signal before noise cancellation. Red: NMR signal after adaptive noise cancellation using two reference coils.

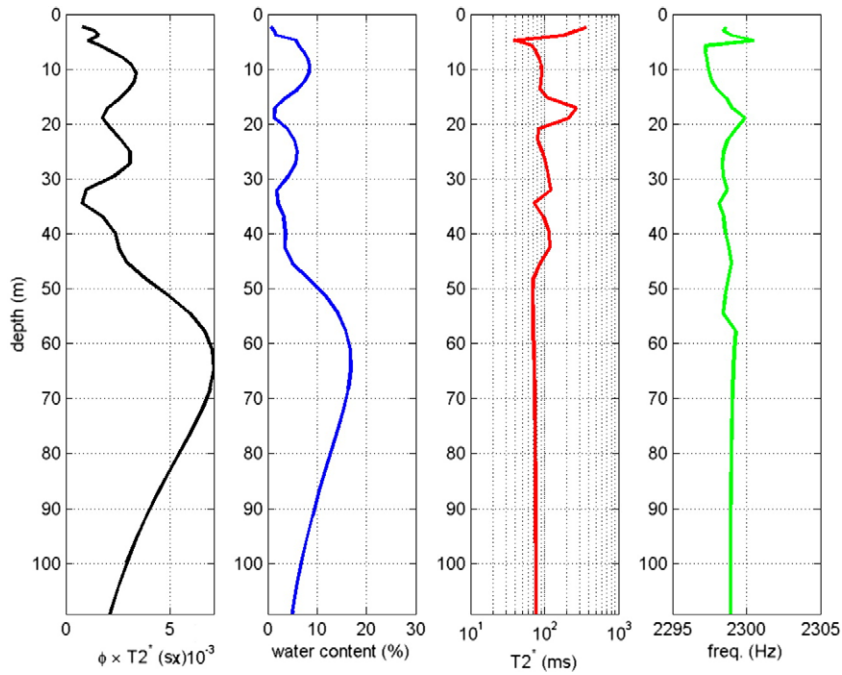


Fig. 4. 1D inversion from USGS site 38 in central Nebraska, USA, April 2007. This inversion was performed on data after adaptive noise cancellation. Black: FID time-domain integral (low-SNR permeability indicator). Blue: NMR-detectable water content. Red: T_2^* . Green: NMR frequency of estimated exponential FID signal. This result is consistent with logs of nearby wells, with a multi-layered sand and silt aquifer above 40 m, and a highly permeable segment of the Ogallala formation below 40 m. (For interpretation of the references to color in this figure legend, the reader is referred to the web version of this article.)

Kooman's (2003) report tested the reliability of an adapted Kozeny–Carmen equation

$$k = C \phi_{\text{NMR}}^4 T_d^2 \quad (15)$$

with laboratory NMR measurements of synthetic and natural porous unconsolidated samples and reported fairly good correlation between measured and NMR-predicted permeability of synthetic samples, but reported very large deviations (up to 2 orders of magnitude) between measured and NMR-predicted permeability for natural samples. The large

deviations for predicted permeability in natural samples was attributed to the effects of paramagnetic materials in the natural samples – effects that are expected to have a much stronger influence at 2 MHz than at 2 kHz.

Lubczynski and Roy (2003) cite a generic empirical formula for permeability derived from surface NMR-based estimates of porosity and T_1 or T_2^* :

$$k = C \phi_{\text{MRS}}^m T_d^n \quad (16)$$

where C , m and n are site specific parameters to be calibrated in the field against K values obtained via pumping tests. As part of his long

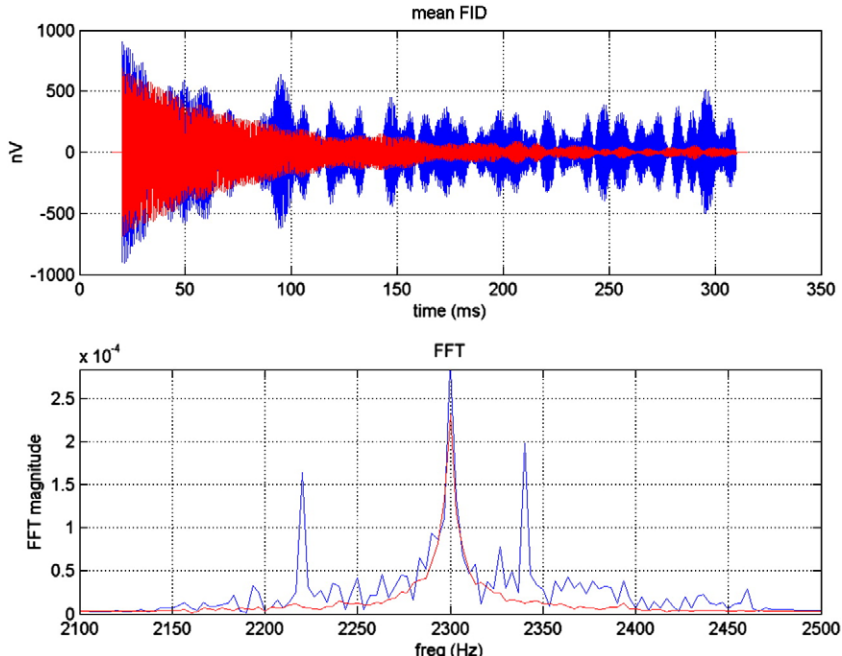


Fig. 5. Surface NMR signal and noise acquired at USGS site 71, in central Nebraska, USA, April 2007. Shown are the mean FID averaged over 64 individual data records with different pulse moments (top), and its frequency spectra (bottom). Blue: NMR signal before noise cancellation. Red: NMR signal after adaptive noise cancellation using two reference coils.

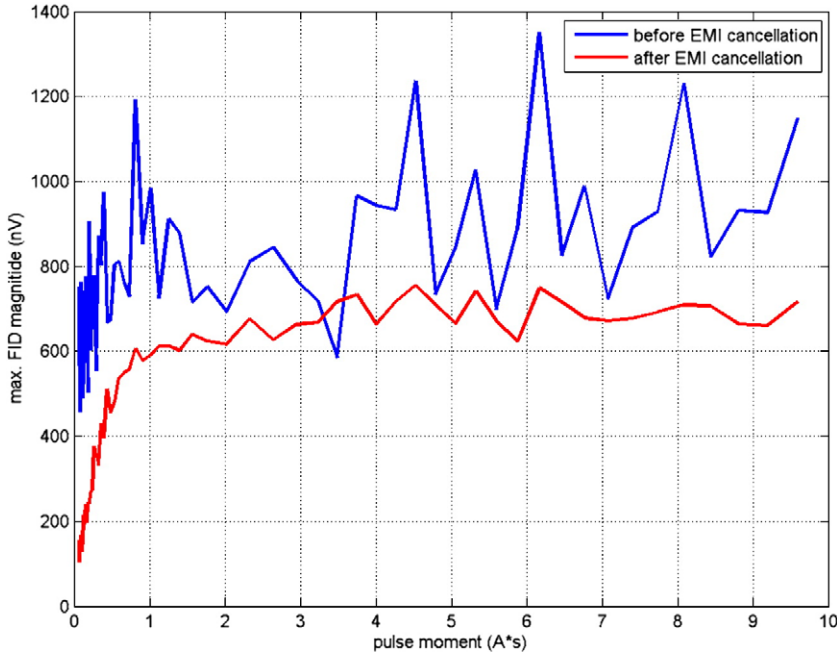


Fig. 6. Maximum signal magnitude vs. pulse moment for USGS site 71 in central Nebraska, USA, April 2007. Blue: NMR signal before noise cancellation. Red: NMR signal after adaptive noise cancellation using two reference coils.

and valuable work in the development of the surface NMR technique, Legchenko et al. (2002) compared aquifer transmissivity measurements with MRS-derived transmissivity estimates based on various combinations of the parameters C , m , n and d in Eq. (16). Legchenko reported the best correlation was obtained using T_1 measurements ($d=1$) with the exponents $m=1$ and $n=2$. A contemporaneous analysis of NMR measurements of unconsolidated glacial rocks (Yaramancı et al., 2002) reported that the exponent $n=4$ provided best fit between NMR-predicted permeability and measured permeability.

It is well known and accepted that the T_2^* relaxation constant can be dominated by the effects of paramagnetic rocks and materials, and

hence T_2^* is a poor indicator of pore size distributions and permeability when paramagnetic effects dominate the T_2^* decay rate. However there is scant published research on the hydrogeologic conditions, specifically the types of and sizes of paramagnetic rocks and grains and the amount of such paramagnetic material present, under which the T_2^* measurement fails as an acceptable substitute for T_2 . Muller (2003) compared 2 kHz surface NMR T_2^* relaxation data originally compiled by Shirov et al. (1991) with laboratory measurements of T_2 relaxation rates at 2 MHz and reported close agreement between the two measurements across a wide range of grain sizes. The two measurements were reported to be approximately equal for grain sizes smaller than fine sand, and for

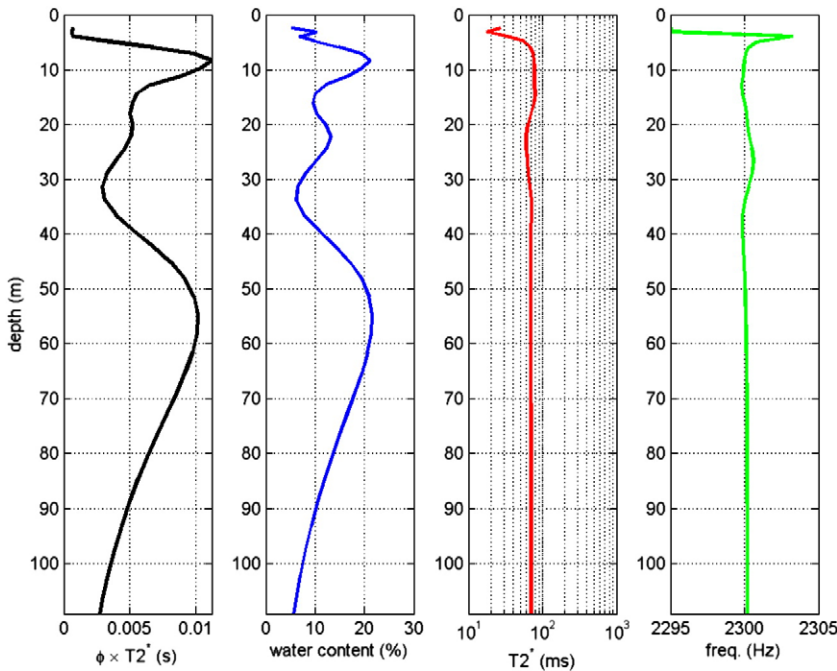


Fig. 7. 1D inversion from USGS site 71 in central Nebraska, USA, April 2007. This inversion was performed on data after adaptive noise cancellation. Black: FID time-domain integral (low-SNR permeability indicator). Blue: NMR-detectable water content. Red: T_2^* . Green: NMR frequency of estimated exponential FID signal. This result is highly consistent with the log of a test well that was subsequently drilled at this site (see Table 1). (For interpretation of the references to color in this figure legend, the reader is referred to the web version of this article.)

larger grain sizes the T_2 measurements at 2 MHz were larger than the T_2^* measurements at 2 kHz by a factor of 1.5–2 (Muller, 2003). More investigation on the use of T_2^* for pore size and/or permeability estimation in surface NMR is certainly warranted.

In summary, we propose using the square of the time-domain integral of the demodulated surface NMR FID signal as an indicator of permeability, and particularly where low SNR prevents reliable estimation of the initial FID amplitude and T_2^* or T_1 decay constants. This integral is proportional to the product of NMR-detected water content and T_2^* , and its square completes the generic model of Eq. (16) with $m=2$, $n=2$, and T_2^* substituted for T_2 . Previous empirical studies of surface NMR-based permeability estimation have suggested values for the exponent m between 1 and 4, and the exponent n between 2 and 4, so this formulation happens to fall in between previously proposed models for the exponents. A similar time-domain integration technique is currently used as a low-SNR permeability indicator in borehole NMR. The dependence of this technique on the T_2^* relaxation process certainly limits the validity of this technique to environments where the influence of magnetic field gradients is small compared to surface relaxation mechanisms. In our experience, this time-domain integral is sometimes the only reliable hydrological parameter that can be derived from very noisy surface NMR data, and as such it merits further evaluation.

3. Results

The results presented here were produced in cooperation with the US Geological Survey, as part of two regional groundwater investigations in central Nebraska (2007) and near San Antonio Texas (2008), USA. All experiments used the GeoMRI system shown in Fig. 1. The 2D imaging results presented here were produced by transmitting on one coil at a time, using a total of 3 transmit coils in sequence. All 1D and 2D inversions assumed an insulating Earth model.

The hydrology in the central Nebraska study area is characterized by the highly productive Ogallala formation (semi-consolidated sandstone, with interbedded sand, gravel and claystone), which is overlain by unconsolidated alluvial deposits in the upper near surface (including interbedded layers of clay, silt, sands and gravels). The data from the Nebraska study are used here to demonstrate adaptive noise cancellation, our proposed 2-step 1D inversion approach, fid integration for low-SNR permeability imaging, and the apparent ability to detect saturated silt/clay units using a reduced dead-time of 15 ms.

The hydrology in the San Antonio TX study area is predominantly karst, with different limestone formations exhibiting different pore size distributions and permeability. A primary objective of the San Antonio study was to identify localized flow paths within and between the various limestone formations. The data from the San Antonio study are used here to demonstrate the utility of adaptive noise cancellation, and the efficacy of our 2D imaging approaches.

3.1. Central Nebraska (April 2007)

The data for these two examples were collected in April 2007, in central Nebraska, USA. In both cases a 91 m (300 ft) square coil was used for detection and 1D NMR profiling.

3.1.1. USGS site 38

The first example was at a site adjacent to a large commercial feedlot (USGS site 38). An electric fence and a single-phase power line ran along the western edge of the feedlot, within 150 m of the eastern edge of the detection coil. A larger 3-phase powerline was located approximately 300 m south of the detection coil, running parallel to a main road. Two reference coils were deployed. A 91 m square reference coil was deployed to the south of the detection coil, towards the large 3-phase power line, with 100 m separation between the closest edges of the two coils. A second, smaller reference coil, approximately 45 m per side, was deployed to the east of the detection coil to within 20 m of

the feedlot, with approximately 100 m separation between the closest edges of the detection and reference coils.

Raw data were acquired using a 40 ms transmit pulse with a 15 ms measurement dead-time, over 64 pulse moments (max. pulse moment ~12 A s), with 16 stacks per pulse moment. Data collection required approximately 2 1/2 h. The data were truncated to a length of 300 ms and digitally filtered to a bandwidth of 200 Hz. A minority (~25%) of individual data records had large impulse noise artifacts and were manually identified and excised. An adaptive processing algorithm was applied, using the data on the two reference channels to cancel noise on the detection channel.

A plot of the mean FID and its frequency spectrum at USGS site 38, averaged over one set of 64 pulse moments (stacking number=1, total acquisition time ~8 min) is shown in Fig. 2, with the blue trace representing the detection channel before adaptive noise cancellation and the red trace represents the same data after adaptive noise cancellation. The broadband noise is clearly reduced by more than one order of magnitude. The FID signal and its spectral peak at 2300 Hz are completely undetectable before adaptive noise cancellation, and are clearly evident after the noise has been cancelled. A plot of the maximum signal amplitude vs. pulse moment, after averaging over 16 stacks, is shown in Fig. 3, before and after adaptive noise cancellation.

A 1D inversion from USGS site 38, using the inversion approach described in Section 2.3, after adaptive noise cancellation and with a stacking number of 16, is shown in Fig. 4. The trace on the left is the time-domain integral of the demodulated FID signal, which as described

Table 1
Drilling log from USGS site 71

Meters	Description
0–0.5	Topsoil
0.5–3.5	Silt, clay, calcite modules, siltstone
3.5–15	Sand, gravel
15–17	Sand, gravel, silt, clay
17–17.5	Silty clay, gravel wash
17.5–18	Sandstone, very fine gravel, gravel wash
18–20	Interbedded silt, sandstone, siltstone
20–24	Silty clay, interbedded sandstone, sticky silt, rootlets
24–27.5	Fine clay, sand, fine to coarse gravel
27.5–30.5	Sandstone, very fine to fine slate stone
30.5–38	Sandstone, very fine to fine
38–39.5	Sandstone, hard, silicon cement, some limey layers
39.5–41.5	Gravel, fine to coarse sand
41.5–44	Fine to coarse gravel
44–47.5	Fine to coarse gravel, cemented layer
47.5–49	Interbedded siltstone – hard, sandstone – hard
49–52	Gravel
52–67	Sandstone, very fine gravel, trace of rootlets, fine sand
67–74.5	Sand, Sandstone, very fine to very coarse, trace of fine gravel
74.5–77	Sandstone, very soft, interbedded with claystone and siltstone
77–79	Siltstone w/ interbedded clay, siltstone
79–81	Silt interbedded w/ clay
81–82	Silt interbedded w/ clay, very fine to moderate sand
82–84.5	Sandstone, very fine to fine, trace of rootlets, soft to med silt
84.5–89	Sand very fine to very coarse, sandstone very fine to very coarse, trace of clay
89–91.5	Sandstone, very fine to fine, trace of clay
91.5–94.5	Sandstone, very fine to medium, trace coarse to very coarse, silt, siltstone, claystone
94.5–96.5	Sandstone, very fine to med, trace of coarse to v. coarse, silt, siltstone, claystone, interbedded
96.5–97.5	Sandstone, v. fine to med, trace of coarse to v. coarse, silt, siltstone, claystone. Silt cemented
97.5–98	Sandstone, very fine, rare very coarse
98–99	Sandstone, v. fine, rare v. coarse, more red claystone
99–100.5	Sandstone, very fine to med, trace very coarse to coarse silt
100.5–102	Sandstone, v. fine to med, trace c. coarse to coarse silt, interbedded claystone, silt and limestone
102–105	Sandstone, med–very sand w/ claystone
105–109.5	Sandstone, med–very sand w/ claystone, very silty
109.5–115	Sandstone, sandy w/ very fine sand
115–127	Siltstone, clay, claystone, black shale

The water table is at approximately 2 m.

earlier is interpreted as a low-SNR permeability indicator. The profiles of water content, T_2^* and NMR frequency were produced via non-linear least squares fitting of a mono-exponential FID model. This inversion result is consistent with logs of nearby wells, which report a multi-layered alluvial sand and silt aquifer above 40 m, and a highly permeable segment of the Ogallala sandstone formation below 40 m. 1D inversions performed on data without adaptive noise cancellation did not produce useful results.

3.1.2. USGS site 71

The second example is from data collected on farmland in the same area of central Nebraska (USGS site 71). The noise level at this site was lower than at the feedlot (USGS site 38), but remained significant. A quick survey with a portable noise measurement device indicated that a power line a few hundred meters north of the site was the dominant noise source. A 91 m (300 ft) square coil was deployed for detection and 1D NMR profiling, and a single 91 m square reference coil was deployed to the north (in the direction of the power line) with approximately 100 m edge-to-edge separation between the detection and reference coils.

Raw data were acquired using a 40 ms transmit pulse with a 15 ms measurement dead-time, over 64 pulse moments (max. pulse moment ~ 12 A s), with 16 stacks per pulse moment. Data collection required approximately 2 1/2 h. The data were truncated to a length of 300 ms and digitally filtered to a bandwidth of 200 Hz. Electric fences (and impulse noise) were not a significant contributor to the noise at this site. An adaptive processing algorithm was applied, using the data on the single reference channel to cancel noise on the detection channel.

A plot of the mean FID and its frequency spectrum at USGS site 71, averaged over one set of 64 pulse moments (stacking number=1, total acquisition time ~ 8 min) is shown in Fig. 5, with the blue trace representing the detection channel before adaptive noise cancellation and the red trace representing the same data after adaptive noise cancellation. The narrowband harmonics of 60 Hz and other broadband noise sources are effectively canceled without distorting the time-domain information of the underlying FID signal. A plot of the maximum signal amplitude vs. pulse moment, after averaging over 16 stacks, is shown in Fig. 6.

A 1D inversion of the data collected at USGS site 71 is shown in Fig. 7. This inversion was performed after adaptive noise cancellation was applied. A test well was subsequently drilled at this site by the USGS (the results of the USGS-directed study will be published by USGS at later date). The predominate grain types noted in the drilling log, summarized in Table 1, are highly consistent with the 1D inversion result shown in Fig. 7.

A second 1D inversion from USGS site 71 was performed using the raw detection coil data without the benefit of adaptive noise cancellation. This inversion, shown in Fig. 8, illustrates two points: 1) Adaptive noise cancellation improves the individual estimates of water content and T_2^* ; 2) the time-domain FID integral (the left most column) maintains its stability and provides a reliable estimate of ϕT_2^* , even when the SNR is too low to reliably estimate ϕ and T_2^* individually.

Fig. 9 shows a plot of the multi-exponential distribution of water content vs. T_2^* and depth at USGS site 71, using the data after adaptive noise cancellation. The features of the multi-exponential distribution also correlate well with the drilling log in Table 1. Specifically the various mixtures of sands, gravels, silts and clays are resolved into as many as 3 distinct T_2^* components for the various layers above 30 m. The concentration of water in the shortest T_2^* bins (10 ms) between 24 m and 32 m correlates with the predominance of clay, silt, and very fine sandstone and slate stone in the drilling log. A variable double porosity response is also evident from 32 m to 75 m, where the drilling log reports complex mixtures of sandstones, sands and gravels.

3.2. San Antonio Texas (January 2008)

A GeoMRI study was conducted in an area of the Edwards aquifer recharge zone, near San Antonio Texas. The objective of this study was to identify shallow groundwater flow paths in valley bottom containing of several distinct limestone formations. A 2D survey was conducted using three square coils, 150 ft (~ 45 m) per side, with each coil having two turns in series. The coil centers were separated by approximately 20 m ($\sim 60\%$ overlap), and the coil array transect was along an exact magnetic E-W line. A fourth surface coil was positioned south of the detection array and used for adaptive noise cancellation.

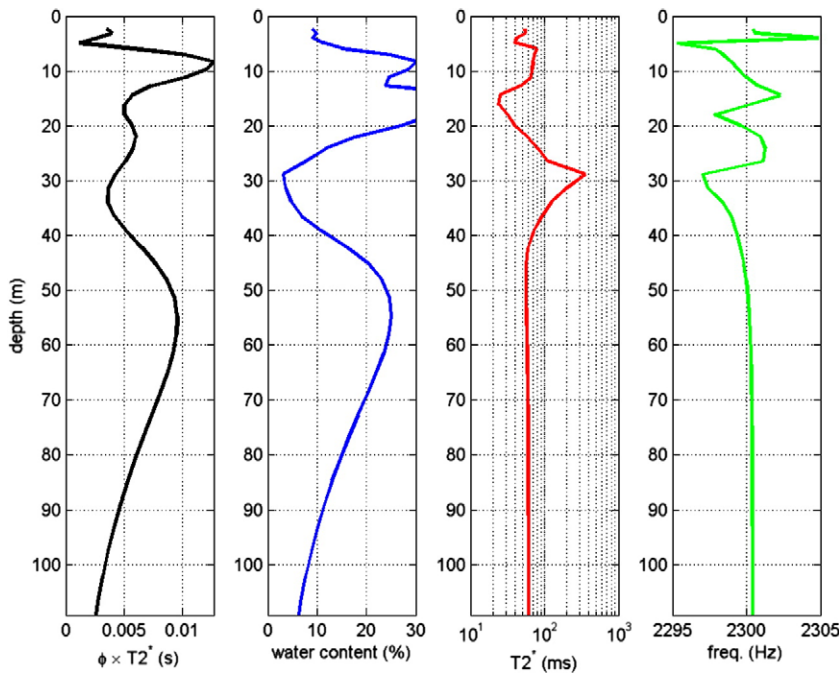


Fig. 8. 1D inversion from USGS site 71 in central Nebraska, USA, April 2007. This inversion was performed on data without the benefit of adaptive noise cancellation. Note that the low-SNR permeability indicator in column 1 is almost identical to the inversion result obtained with higher SNR data (compare to column 1 in this figure), while the non-linear least squares estimates of water content, T_2^* and NMR frequency exhibit instability and increased variance in this low-SNR data.

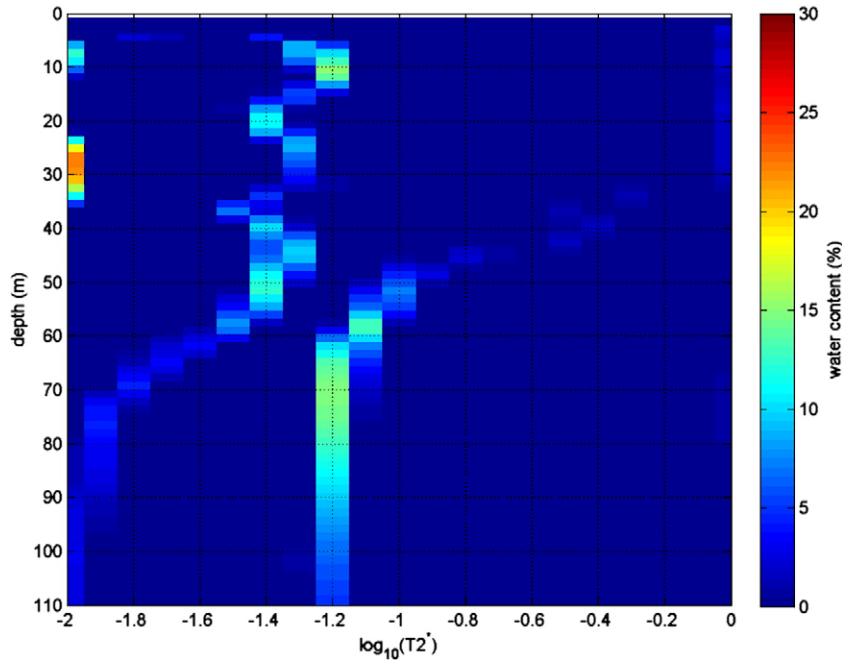


Fig. 9. Multi-exponential distribution of water content vs. $T2^*$ and depth at USGS site 71.

The three single coil 1D inversions (not shown) indicated three distinct formations, with varying NMR signal characteristics. All of the NMR data and interpretations of the valley in MA-7 indicate the presence of three distinct water-bearing formations:

1. An upper unit with water contents ranging from 3%–10% in medium to very large pores from depths of 5 m–13 m. The NMR-detected water in this upper zone might be sitting in the lower, undrainable portions of vugs in the weathered limestone.
2. An intermediate unit with comparatively lower water content and permeability, from 15 m–35 m.
3. A permeable aquifer below 40 m with consistent NMR-detected water content between 5% and 10%. The water content in this lower aquifer is distributed fairly consistently between medium size pores (presumably the microscopic porosity component of saturated limestone) and essentially bulk water (presumably contained in fractures and larger vugs).

The resulting 2D MR images (Figs. 10 and 11) indicated a distinct localized increase in water content and permeability in the intermediate zone, approximately 30 m east of the center of the 2D survey line. This indicates a possible water filled fracture zone or cave, and a potential flow zone between the upper and lower formations at this location. The 2D images, particularly the matched filter image (Fig. 10), also indicate a zone of very low water content on the far west side of the 2D survey line. This corresponds to an electrically-resistive formation identified in a previous Ohm-mapper survey.

4. Conclusions

Multi-channel surface NMR instrumentation and software application offer practical benefits in noise reduction and 2D/3D groundwater profiling.

The combined use of dedicated noise reference coils and adaptive signal processing techniques provides a powerful and robust basis for

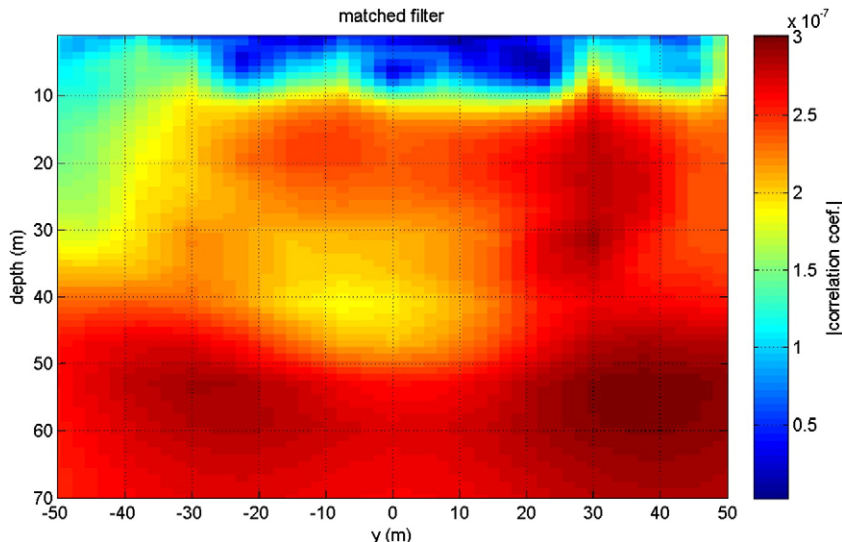


Fig. 10. 2D MR correlation image of study site in San Antonio indicates upper, lower and intermediate water-bearing formations, possible fracture zone or cave between the upper and lower units at $y=+30$ m, and a region of relatively low water content and permeability on the far west side of the survey ($+y$ =magnetic East).

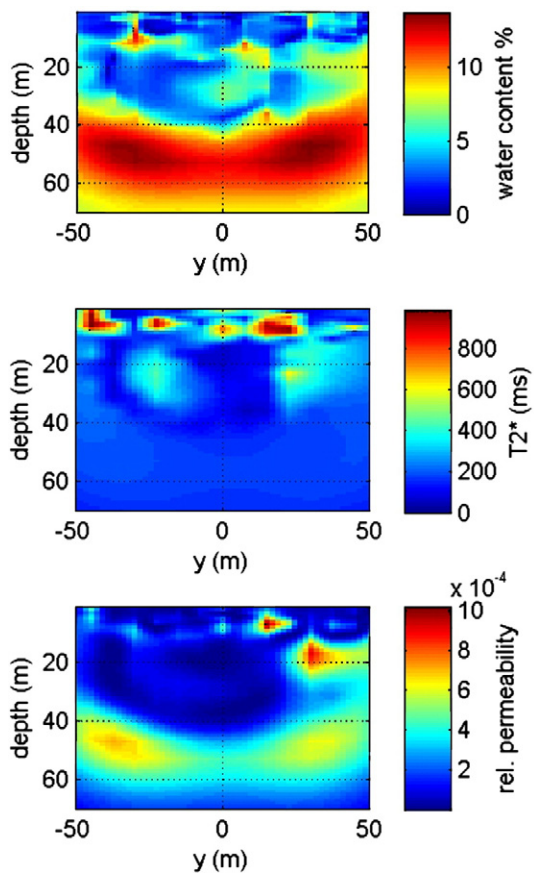


Fig. 11. 2D linear inversion of San Antonio study area (same data as Fig. 10), with individual 2D estimates of water content, T_2^* and relative permeability.

mitigating environmental and cultural noise. In our experience, the use of reference coils and adaptive signal processing typically reduces noise levels by a factor of 5 to 10, and sometimes by a larger factor depending on the level and coherence of the noise source(s). In practice, this broadens the applicability of surface NMR to use in and around developed areas, not just rural areas.

The primary potential pitfall of using dedicated reference coils is that, depending on the position and size of the reference coil(s), it is possible for the reference coil to detect NMR signals from groundwater, and these groundwater signals can be inadvertently added or subtracted to the detection coil data as part of the noise cancellation process. We have observed this numerous times in practice, as have other researchers (Lange et al., 2006). Thus, when using dedicated noise cancellation coils it is advisable to locate the reference coils as far from the transmitting and detecting coils, and as close to the noise source(s) as possible.

2D surface NMR imaging in its current form appears to provide useful and relevant 2D spatial resolution for groundwater development and environmental investigations. The results presented here indicate the ability to resolve localized hydrogeological features on the order of a fraction of the coil diameter. This is consistent with recent numerical modeling and field experience in 2D surface NMR spatial resolution (Hertrich and Yaramanci, 2006). This 2D resolving capability is expected to particularly benefit investigations of highly heterogeneous water-bearing formations in the near surface.

The extension of the 2D surface NMR technique to 3D has been previously demonstrated in computer modeling and small-scale laboratory experiments (Walsh, 2006). Practical 3D surface NMR field investigations will likely benefit from the development of instrumentation with even more channels (i.e. 8 or 12 Tx/Rx channels).

Acknowledgments

This work was supported by the National Science Foundation under Grant #0450164. Any opinions, findings, and conclusions or recommendations expressed in this material are those of the author and do not necessarily reflect the views of the National Science Foundation.

Special thanks to Mr. Erik Magnuson, Dr. Geoff Barrall and Mr. Dave Skvortz of GE Security in San Diego CA, and Mr. Michael LaFrance of Lewis Bass International in Campbell CA, for their invaluable assistance in the design and manufacture of the GeoMRI power electronics. The author also thanks the following persons and organizations for their assistance in the initial field testing of the GeoMRI instrument in 2006 and 2007: US Geological Survey, US National Park Service, Nebraska Department of Natural Resources, University of Iowa, University of Minnesota, Iowa State University, Stanford University, University of Texas at El Paso, the Pacific Northwest National Laboratory, and Mr. John Ackerman.

References

- Allen, D., et al., 2000. Trends in NMR logging. *Oilfield Review* 2–20 Autumn.
- Braun, M., Hertrich, M., Yaramanci, U., 2005. Study on complex inversion of magnetic resonance soundings. *Near Surface Geophysics* 3 (3), 155–164.
- Haykin, S., 1996. *Adaptive Filter Theory*. Prentice Hall, Upper Saddle River, New Jersey.
- Hertrich, M., Yaramanci, U., 2003. Surface NMR with separated loops – investigations on spatial resolution. Proc. of the 2nd International Workshop on the MRS Method, November 2003, pp. 41–44.
- Hertrich, M., Yaramanci, U., 2006. Magnetic resonance sounding data inversion. Proc. of the 3rd Magnetic Resonance Sounding International Workshop, October 2006, pp. 15–20.
- Hertrich, M., Braun, M., Yaramanci, U., 2005. Magnetic resonance soundings with separated transmitter and receiver loops. *Near Surface Geophysics* 3 (3), 141–154.
- Kenyon, W.E., 1992. *Nuclear Geophysics* 6 (2), 153–171.
- Kenyon, W.E., Gubelin, C.M., 1995. Nuclear magnetic resonance imaging – technology for the 21st century. *Oilfield Review* 19–33 Autumn 1995.
- Kooman, S., 2003. Saturated hydraulic conductivity derived from (hydro)geophysical measurements, MSc. Thesis, Wageningen University, NL, 2003.
- Lange, G., Meyer, R., Di Battista, M., Muller, M., 2006. Loop configurations experiments on multiple layered primary aquifers in South Africa and Germany. Proc. of the 3rd Magnetic Resonance Sounding International Workshop, October 2006, pp. 69–72.
- Legchenko, A., 2006. MRS measurements and inversion in presence of EM noise. Proc. of the 3rd Magnetic Resonance Sounding International Workshop, October 2006, pp. 21–24.
- Legchenko, A., Shushakov, O., 1998. Inversion of surface NMR data. *Geophysics* 63 (1), 75–84.
- Legchenko, A., Valla, P., 2003. Removal of power-line harmonics from proton magnetic resonance measurements. *Journal of Applied Geophysics* 53, 103–120.
- Legchenko, A., Baltassat, J.M., Beauché, A., Bernard, J., 2002. Nuclear magnetic resonance as a geophysical tool for hydrogeologists. *Journal of Applied Geophysics* 50, 21–46.
- Li, Z., Zeng, L., Pan, Y., Wang, P., 2006. The attempt of wavelet analysis applied to improving S/N ratios of MRS signal. Proc. of the 3rd Magnetic Resonance Sounding International Workshop, October 2006, pp. 61–64.
- Lubczynski, M., Roy, J., 2003. MRS contribution to hydrogeological parameterization. Proc. of the 2nd International Workshop on the MRS Method, November 2003, pp. 73–76.
- Mohnke, O., Yaramanci, U., 2003. Spectral inversion and interpretation of surface nuclear magnetic resonance data. Proc. of the 2nd International Workshop on the MRS Method, November 2003, pp. 81–84.
- Mohnke, O., Yaramanci, U., 2005. Forward modelling and inversion of MRS relaxation signals using multi-exponential decomposition. *Near Surface Geophysics* 3 (3), 165–186.
- Muller, M., 2003. Dispersion of Nuclear Magnetic Resonance (NMR) relaxation. 20 Kolloquium Electromagnetische Tiefenforschung, Königstein, Sep 29–Oct 3, p. 2003.
- Sen, P.N., Straley, C., Kenyon, W.E., Whittingham, M.S., 1990. Surface to volume ratio, charge density, nuclear magnetic relaxation and permeability in clay bearing sandstones. *Geophysics* 55 (1), 61–69.
- Sezginer, A., Cao minh, C., Heaton, N., Herron, M., Freedman, R., Van Dort, C., 1999. An NMR high-resolution permeability indicator. *Transactions of the SPWLA 40th Annual Logging Symposium*, Oslo, Norway, May 1999.
- Shirov, M., Legchenko, A., Creer, G., 1991. A new direct non-invasive groundwater detection technology for Australia. *Exploration Geophysics* 22, 333–338.
- Strehl, S., Rommel, I., Hertrich, M., Yaramanci, U., 2006. New strategies for filtering and fitting of MRS signals. Proc. of the 3rd Magnetic Resonance Sounding International Workshop, October 2006, pp. 65–68.
- Walsh, D.O., 2006. Multi-channel MRS instrumentation and software for enhanced noise mitigation and 2D/3D imaging. Proc. of the 3rd Magnetic Resonance Sounding International Workshop, October 2006, pp. 73–76.
- Yaramanci, U., Lange, G., Hertrich, M., 2002. Aquifer characterization using surface NMR jointly with other geophysical techniques at the Nauen/Berlin test site. *Journal of Applied Geophysics* 50, 2002, 47–65.